ACS OMEGA

http://pubs.acs.org/journal/acsodf Article

Complementary Adsorption of Binary Levelers for Highly Uniform Cu Micropillars

Yugeun Jo, Sung-Min Kim,* SangHoon Jin, Woon Young Lee, Sang-Yul Lee,* and Min Hyung Lee*

Cite This: *ACS Omega* 2022, 7, 36880−36887 Read Online

ACCESS | Metrics & More | Article Recommendations | Supporting Information

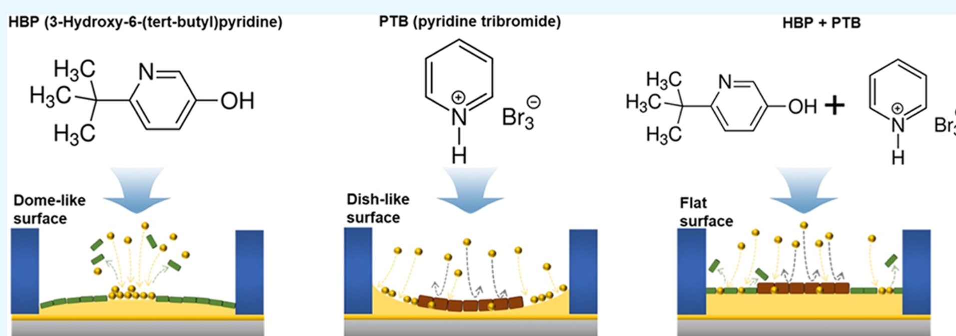

ABSTRACT: Highly uniform Cu micropillars were electrodeposited on a Cu seed layer in a micropatterned photoresist in the presence of binary levelers containing pyrrolidine and pyridine functional groups. The adsorption behaviors of binary levelers, i.e., 3-hydroxy-6-(*tert*-butyl)pyridine and pyridinium tribromide in an electroplating bath were investigated by chronopotentiometry with sequential injection of levelers and linear sweep voltammetry with a rotating disk electrode. From electrochemical analysis, pyridinium tribromide composed of a positively charged pyridine ring was strongly adsorbed on the Cu seed surface, relative to 3-hydroxy-6-(*tert*-butyl)pyridine. Additional microscopy, surface roughness, and nitrogen concentration analyses revealed that the binary levelers were preferentially adsorbed on the center and the edge region of the Cu seed, resulting in a uniform Cu pillar profile. The possible mechanism of highly uniform Cu pillar deposition was discussed in terms of the adsorption behaviors of the levelers dependent on their molecular structures.

1. INTRODUCTION

Flip-chip technology has been widely used in semiconductor packages on the basis of its small form factor, high-frequency operation, and high I/O density.[1,2] Copper (Cu) micropillar bumps in miniaturization of the flip chips can enable a finer pitch and reduced die size.[2] In fine pitch, a uniform profile of Cu pillars has been critical for ensuring good electrical connections and reliability of the solder joint, since poor coplanarity of Cu pillars results in short circuits or irregular bumps in the solder bonding process.[3] Many factors influencing Cu electrodeposition related to inorganic-based electrolyte chemistry, organic additive species, applied current density, and the bath convection environment have been reported in the context of achieving uniform pillar shape.[3−6] In particular, organic additives in the plating bath play a very important role in controlling the shape and coplanarity of deposited Cu pillars.[7]

To ensure good electrical connections and reliability of the solder joint, the coplanarity of Cu pillars is controlled through the synergistic effect of three additives: an accelerator, a suppressor, and a leveler.[4,5,8] Typically, bis-(sodium sulfopropyl)-disulfide (SPS) as an accelerator and poly(ethylene glycol) (PEG) as a suppressor are basic additives that have been reported in multiple studies.[9,10] Levelers composed of specific chemical structures containing nitrogen could be preferentially adsorbed on the protrusions of the substrate on which the current concentrates, since the positively charged nitrogen-based functional groups of levelers are electrostatically attracted. Through such a process, the uniform surface can be achieved by the increase in overpotential on the protrusion and prevention of Cu deposition. As well known, the most commonly used levelers in Cu electroplating are amine functionality such as polyethyleneimine (PEI)[11,12] and quaternary ammonium compounds such as Janus Green B and Diazine Black.[13−15] Some previous works suggested that the amine functional group plays an important role in the leveler by preferentially adsorbing on the areas strongly affected by electric fields when the high current density is

Received: August 31, 2022
Accepted: September 28, 2022
Published: October 5, 2022

ACS Publications © 2022 The Authors. Published by American Chemical Society

applied.[16,17] In contrast, quaternary ammonium with the only nitrogen cation with a permanent positive charge is able to be also adsorbed onto the restricted area by a high electric field and block electrodeposition by electrostatic attraction, resulting in a leveling effect on the substrate.[16] However, it should be noted that the planarization of Cu electroplating is clearly beyond the commonly used leveler, since in most of the cases, electroplated Cu micropillars have a domed or dished surface rather than a flat topography.[5]

Herein, we designed novel binary levelers having pyrrolidine and pyridine structures to realize Cu micropillars with uniform thickness and a flat surface. 3-Hydroxy-6-(*tert*-butyl)pyridine (HBP) and pyridinium tribromide (PTB) were adopted on the basis of their different adsorption behaviors. HBP composed of polar functional groups, such as hydroxyl or carbonyl groups, prevented excessive inhibition of Cu deposition by the weak adsorption on the cathode surface,[18] while another cationic leveler PTB containing positively charged nitrogen[19] promoted strong adsorption on the center area of the cathode, i.e., the electric-field-concentrated region. Therefore, simultaneous use of two levelers enabled a flat surface to be realized on the Cu micropillars, as evidenced by the microscopy results. Furthermore, to scrutinize the adsorption behaviors of the two levelers, atomic force microscopy, galvanostatic potential transient measurements, and secondary ion mass spectrometry were carried out. This study provides a strategic approach to prepare highly uniform Cu micropillar bumps for scientific and practical advances in semiconductor fields.

2. EXPERIMENTAL DETAILS

2.1. Chemicals. Cupric sulfate pentahydrate ($CuSO_4 \cdot 5H_2O$), sulfuric acid (H_2SO_4), and hydrochloric acid (HCl) were supplied from Daejung Chemicals. Bis-(sodium sulfopropyl)-disulfide (SPS, $C_6H_{12}Na_2O_6S_4$) was purchased from Alfa Chemistry. 3-Hydroxy-6-(*tert*-butyl)pyridine (HBP, $C_9H_{13}NO$), pyridinium tribromide (PTB, $C_5H_6Br_3N$), and poly(ethylene glycol) (PEG, $H(OCH_2CH_2)_nOH$, MW: 4000) were purchased from Sigma-Aldrich.

2.2. Cu Pillar Electroplating. To prepare a semiconductor-grade bump patterned wafer, Ti with a thickness of 50 nm as a barrier layer and Cu with a thickness of 1 μm as a seed layer were deposited by the physical vapor deposition (PVD) process. The photoresist (PR) for a bump with a diameter of 50 μm and a height of 50 μm was patterned by chemical development after photosensitization using an ultraviolet beam lithography system (JBX-9300FS, JEOL Ltd.), as shown in Figure S1.

The Cu electroplating bath was 160 g/L $CuSO_4 \cdot 5H_2O$, 140 g/L H_2SO_4, and 50 mg/L Cl^-. PEG and SPS were added to the Cu bath as a suppressor and an accelerator, respectively. The concentrations of PEG and SPS were, respectively, fixed at 150 and 15 mg/L in all experiments. This Cu bath is denoted in the following as the base solution (BS). In addition to the BS, two different levelers of 20 mg/L HBP and 20 mg/L PTB were simultaneously added for the coplanarity of the Cu micropillars, and their molecular structures are shown in Figure 1. The Cu electrodeposition was conducted using a three-electrode system (VersaSTAT3, Princeton Applied Research) in the BS containing different levelers such as HBP, PTB, and coaddition of HBP and PTB. To achieve a 30 μm thickness of the Cu pillars, a current density of 50 mA/cm^2 was applied for 1628 s.

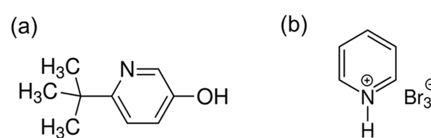

Figure 1. Molecular structures of (a) HBP and (b) PTB.

2.3. Electric Field Modeling. The electric field distribution in the PR was modeled by means of simulation software (Quickfield 6.0, Tera Analysis Ltd). With PR geometry with a diameter of 50 μm and a height of 50 μm, the simulation was performed using the electrical conductivity (100 S/m) and temperature (25 °C) of the Cu electrolyte. The potential was fixed at −0.5 V and PR was set as a nonconductor (E = 0 V).

2.4. Morphology and Physical Characterization. After electroplating, the surface morphology and coplanarity of the Cu pillar were characterized by a confocal laser scanning microscope (CLSM, LEXT OLS4100, Olympus) and by a field emission scanning electron microscope (FE-SEM, JSM-7001F, JEOL). Based on cross-sectional profiles obtained by a CLSM, the nonuniformity of Cu pillars using randomly selected five pillars was calculated according to the following equation

$$\text{non} - \text{uniformity}\ (\%) = \frac{\text{maximum thickness} - \text{minimum thickness}}{2 \times \text{average thickness}} \times 100 \quad (1)$$

The morphology and surface roughness of the Cu deposits were examined with an atomic force microscope (AFM, XE-100, Park System). Nitrogen incorporated into the Cu electrodeposit dependent on the levelers was determined by secondary ion mass spectrometry (SIMS, PHI 6300, Physical Electronics). The coordinate of the center and the edge on the Cu pillar surface was carefully assigned to rule out the interference zone (ca. 10 μm) by sputtering. The average concentration of nitrogen was calculated at a depth profile range from 5 to 10 μm Cu electrodeposited depth.

2.5. Electrochemical Measurements. The adsorption kinetics dependent on the chemical species of levelers were evaluated by chronopotentiometry and LSV (linear sweep voltammetry). In the chronopotentiometry test, a constant deposition current density of 50 mA/cm^2 was applied for 540 s. To reflect the adsorption behaviors of HBP and PTB, the potential transients for the patterned wafer and bared wafer were monitored after injection of one leveler at 180 s and subsequent injection of another leveler at 360 s. In the case of LSV, the analyses were conducted with a three-electrode system containing a photoresist-patterned wafer (geometric area = 1.5 × 1.5 cm^2) as the working electrode, a Pt-coated Ti wire as the counter electrode, and a saturated sulfate electrode (SSE) as the reference electrode. The LSV was recorded by sweeping from 0 to −0.8 V at a scan rate of 10 mV/s, and the rotation rate of the rotating disc electrode (RDE) was changed from 400 to 1000 rpm.

The adsorption kinetics of HBP, PTB, and binary HBP + PTB were evaluated by an electrochemical quartz crystal microbalance (EQCM). The BS was used as the electrolyte, which was the same solution used for Cu pillar electroplating. EQCM measurements were performed using a potentiostat (VersaSTAT III, PAR) equipped with a QCM922 module (QCM922, Princeton Applied Research). The quartz crystal frequency and current density were 9.04 MHz and 50 mA/

https://doi.org/10.1021/acsomega.2c05646
ACS Omega 2022, 7, 36880−36887

cm^2, respectively. The nonpatterned flat Cu electrodes with an active surface area of 0.198 cm^2 were used as substrates.

3. RESULTS

The Cu pillars are formed on the Cu seed layers in the bottom of the photoresist holes. As shown in Figure 2, the electric field tends to be only concentrated on the center of the seed layer due to the high and narrow architectures as well as the hydrophobicity of the photoresist. Typically, the convex pillar shape is obtained due to the preferential Cu deposition on the center of the seed by the concentrated electric field. To achieve a uniform top surface of the pillars, Cu deposition should be adequately inhibited at the center region, where the current flux is concentrated.[16,20] As well known, levelers play an important role in the inhibition of Cu deposition due to their strong adsorption on the current-concentrated center region. Thus, we adopted levelers with a pyridine functional group and an *N*-quaternized pyridine group, exhibiting different adsorption behaviors, and experimentally scrutinized the uniformity of the Cu pillars.

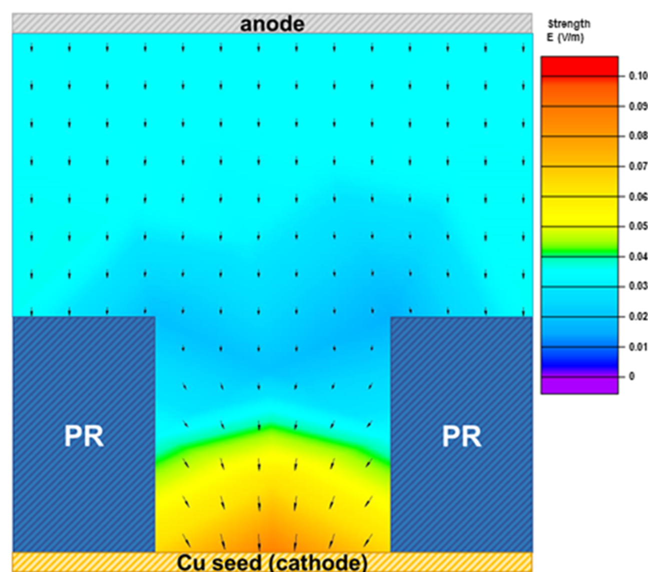

Figure 2. Simulation of the electric field in the photoresist-patterned wafer using Quickfield software.

To obtain a uniform profile of Cu pillars, Cu electrodeposition was conducted with different levelers, i.e., HBP, PTB, and a binary combination of HBP + PTB. As shown in Figure 3a,e, the Cu pillar electroplated in the absence of a leveler shows a dome-like shape with a nonuniform thickness (ca. 11%). As expected, this is due to the fact that the transfer of Cu cations was concentrated on the center region rather than being uniformly distributed on the entire surface of the Cu seed layer. The pillar shape in the presence of HBP also showed a similar dome-like tendency of BS despite a decrease in nonuniformity (6.3%) relative to the BS (Figure 3b,f). Presumably, the weak adsorption of the HBP's functional group on the center region might lead to a convex shape. In contrast, as can be seen in Figure 3c,g, the dish-like shape was observed in the presence of PTB, which could be attributed to the preferentially strong adsorption on the electric-field-concentrated center region. To verify the shape of Cu pillars, we further carried out the electrodeposition with various concentrations of each leveler. As shown in Figure S2, the convex and concave shapes were maintained without a significant change in the thickness uniformity, although the concentrations of HBP and PTB were varied, respectively. In the case of the coaddition of HBP (20 mg/L) and PTB (20 mg/L), a highly uniform surface was obtained as evidenced by a nonuniformity value of ca. 2.6% (Figures 3d,h and S3). The possible mechanism of the formation of uniform Cu pillars in the presence of binary levelers is comprehensively discussed below.

According to results of top-view microscopy and surface roughness, as shown in Figure 4, it was found that the *Ra* values as the arithmetic mean surface roughness in the presence of levelers were more than 2-fold smaller in comparison to BS. This is due to the fact that the levelers adsorbed on the Cu surface inhibited Cu growth, resulting in a grain refinement effect.[13,21,22] The center and edge roughness of the Cu pillars were also measured to examine the adsorption behaviors dependent on the electric field influence. Interestingly, HBP showed almost identical *Ra* values regardless of the

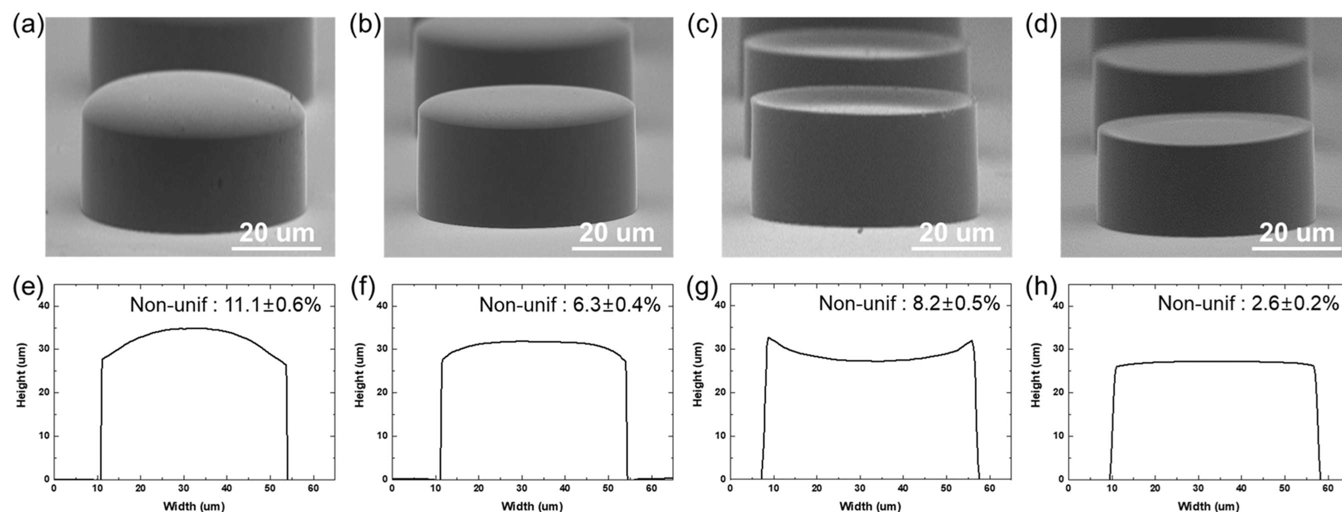

Figure 3. FE-SEM tilted view and cross-sectional profile of Cu pillars obtained using (a, e) BS, (b, f) HBP, (c, g) PTB, and (d, h) binary HBP + PTB.

https://doi.org/10.1021/acsomega.2c05646
ACS Omega 2022, 7, 36880−36887

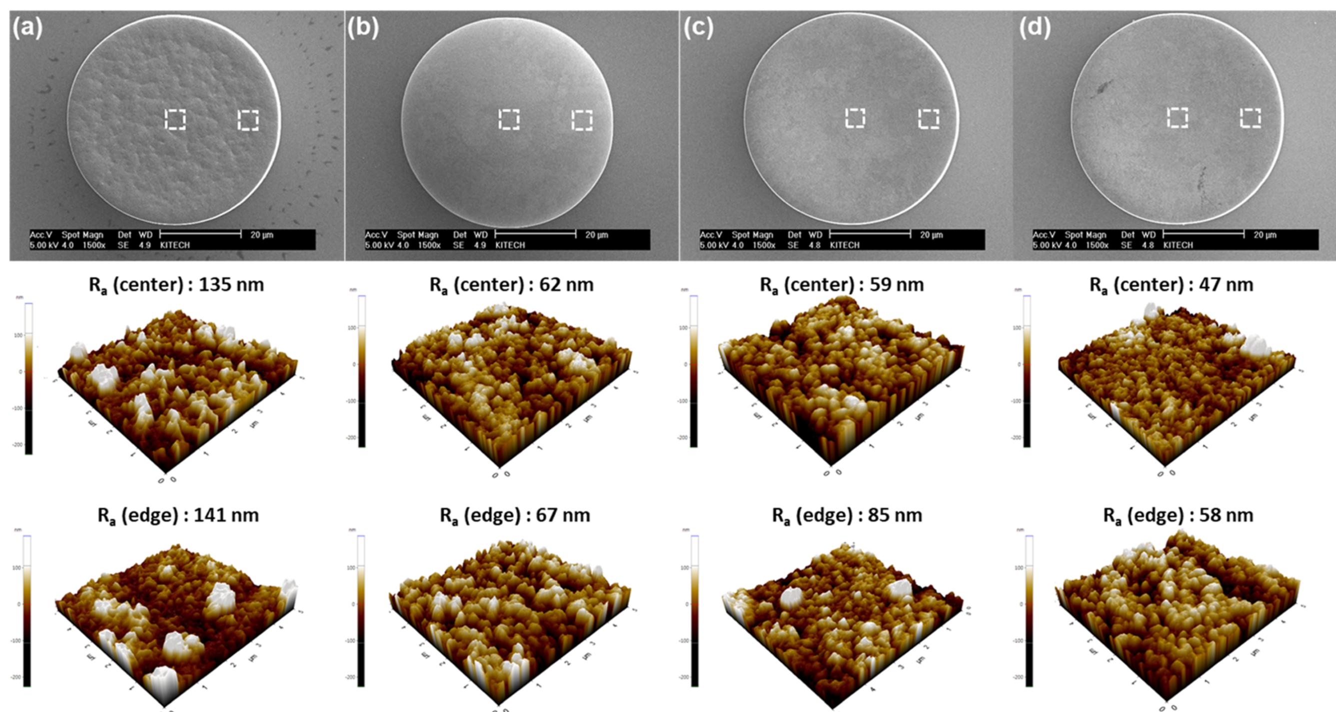

Figure 4. FE-SEM top-view images and AFM topographies corresponding to (a) BS, (b) HBP, (c) PTB, and (d) binary HBP + PTB.

center and edge of the pillars, whereas the *Ra* of the center in the presence of PTB was 26 nm lower than that of the edge (Figure 4b−d). Thus, it could be postulated that PTB was preferentially adsorbed on the center region, as evidenced by tilted FE-SEM and confocal microscopy images exhibiting dish-like concave shape pillars. In the case of the binary combination of HBP + PTB, the *Ra* value was lower in comparison with HBP and PTB and the *Ra* of the center was relatively lower than that of the edge. This could be mainly attributed to the complementary adsorption of binary levelers, in which PTB was strongly adsorbed on the center region during the weak adsorption of HBP on the entire Cu surface.

Chronopotentiometry was monitored to investigate the adsorption behaviors of HBP and PTB for different substrates of a patterned wafer and a bare wafer. Figure 5a shows the corresponding changes in the cathodic potential from sequential addition of HBP and PTB (red line) and PTB and HBP (blue line) during the electrodeposition on the patterned wafers. The potential increased from −0.25 to −0.33 V, following injection of HBP into the leveler-free base electrolyte at 180 s. Sequentially, the potential was further increased up to −0.44 V after PTB was injected into the electrolyte containing HBP at 360 s. In the reverse order of leveler injection, the first injection of PTB resulted in an abrupt increase in the potential up to −0.39 V. The subsequent injection of HBP also led to an increase in the potential value to −0.44 V, identical to the transient potential value of the sequential injection of HBP and PTB. The increased overpotential with addition of PTB can be attributed to the strong adsorption on the Cu surface, which blocks the active sites of the cathodic reactions.[23,24] Consequently, it was found that PTB exhibited a higher potential change in comparison with HBP, suggesting that the adsorption of PTB was stronger than that of HBP. In addition, the same potential value after 360 s regardless of the injection sequence could be ascribed to the different selective adsorption of HBP and PTB. To better

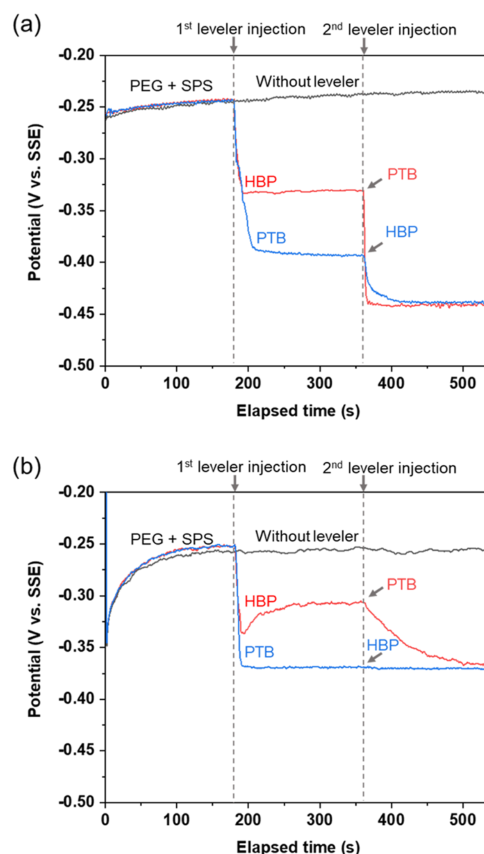

Figure 5. Graph of the measured potential (V) versus time (t) using data collected from experiments performed in BS in which HBP and PTB are sequentially added at 180 and 360 s, respectively, at (a) ø50 μm patterned wafer and (b) 1.5 cm × 1.5 cm bare wafer.

understand the adsorption behaviors of HBP and PTB, chronopotentiometry was further conducted on a bare wafer,

https://doi.org/10.1021/acsomega.2c05646
ACS Omega 2022, 7, 36880−36887

providing a large area that is less affected by the electric field concentration compared to patterned wafers with a complex architecture including photoresists (Figure 5b). As soon as HBP was injected at 360 s, the potential sharply increased to −0.33 V and then slightly decreased until the steady state at ca. −0.31 V was maintained. At 360 s, the subsequent injection of PTB induced a gradual increase in the potential. The result from the injection sequence of HBP and PTB suggested that the functional group of HBP might be adsorbed on the entire Cu surface, as represented by an abrupt increase in potential, and the weak inhibitory effect of HBP led to the growth of Cu deposit during the desorption of HBP, as shown by a slight decrease in potential. As indicated by the gradual increase in the potential after 360 s, PTB appeared to inhibit Cu growth due to its strong adsorption nature. However, in the injection sequence of PTB and HBP, the potential change was not observable despite subsequent injection of HBP after the steep increase in the potential in the presence of PTB. Considering the large area of the bare wafer, it was believed that PTB was strongly adsorbed on the entire Cu surface, since the large area of the bare wafer was affected by the electric field, unlike a patterned wafer. Thus, the constant potential in the injection sequence of PTB and HBP may reflect strong adsorption of PTB on the entire wafer, disabling the weak adsorption of HBP.

To gain insights into the adsorption behaviors in terms of mass transport, LSV on Cu RDE with a rotating speed in the range from 400 to 1,000 rpm was carried out in the presence of HBP and PTB, as shown in Figure 6. It is theoretically and experimentally established that the current density increased with the increase of the rotating speed of RDE due to the mass transfer of cupric ions.[25] From an examination of the LSV curves in the presence of HBP (Figure 6a), similar inhibition effects up to ca. −0.23 V were observable regardless of the rotating speed of the electrodes. However, the current density significantly increased with increasing rotating speed from 400 to 1000 rpm after a potential of −0.23 V. This increase in the current density could originate from the decrease in the surface coverage or weak adsorption of HBP, facilitating Cu deposition. In the case of PTB, the Cu deposition in the highly negative potential region up to ca. −0.53 V was strongly inhibited even at a high rotation rate of the RDE, as revealed by the steadily maintained current density in Figure 6b. Typically, the halide ions such as Cl^- and Br^- can be adsorbed on the Cu seed surface and subsequently form a cuprous electron bridge and binds with PEG. This complex composed of halide and cuprous ions and PEG is adsorbed on the entire surface of the Cu layer and inhibits copper electrodeposition. It was reported that the addition of Br^- with the cationic additive had a stronger inhibitory effect under a rapid convection environment than Cl^-.[26] As a result, a constant potential could be maintained even at a high speed of 1000 rpm by the strong adsorption process of positively charged nitrogen of the quaternary pyridine ring on the center region of the Cu seed surface and the Br−based complex on the entire Cu surface. At a practical current density of 50 mA/cm^2 for the Cu pillar electrodeposit, the potential change calculated to be 16 mV was found to be much lower than the potential change (132 mV) of HBP. It is noticeable that the overpotential should be decreased to cross the reaction barrier to achieve Cu deposition, since the mass transportation of Cu ions was accelerated with an increase in the RDE speed under the same current density, i.e., the same deposition rate. However, the overpotential in the case of PTB was nearly constant, which was explained by the significant suppression of Cu deposition that took place.

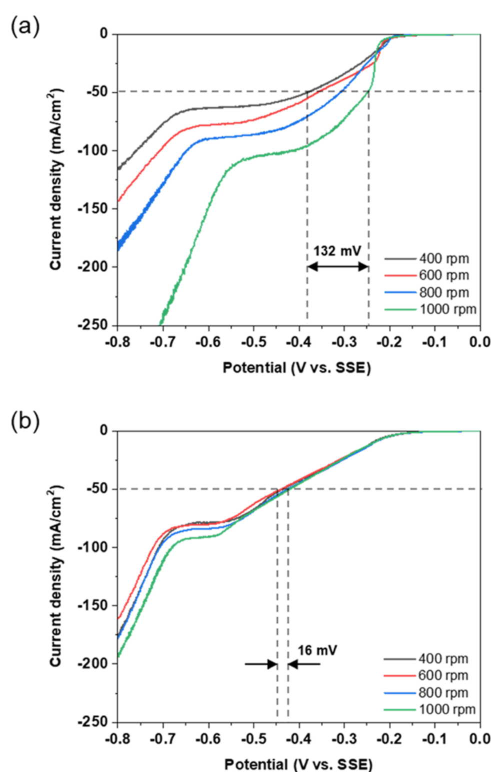

Figure 6. Linear sweep voltammetry curves using a rotating disk electrode in an electroplating solution containing (a) HBP and (b) PTB.

Mass change is an important clue for inferring the adsorption behavior of levelers because the *N*-functional species of levelers adsorbed on the Cu surface could be predicted. Thus, to further elucidate the formation of flat Cu pillars correlated with the adsorption behaviors of HBP and PTB, the mass change was monitored by EQCM, and the mass change of the electrodes (see Figure S4 and Table 1) was converted from the value of the frequency change according to Sauerbrey's equation.[27]

Table 1. Summarized Change in Weight Value Based on EQCM Measurements

conditions	$\Delta mass_{total}$ (μg)	$\Delta mass_{Lev} - \Delta mass_{BS}$ (μg)	adsorption rate (μg/s)
BS	750.68		
HBP	779.07	28.39	0.05
PTB	920.49	169.81	0.31
HBP + PTB	945.85	195.17	0.36

$$\Delta m = \frac{-\Delta freq \times A \times \sqrt{uq \times pq}}{2\,(Fq^2)} \quad (2)$$

where Δm is the mass change, Δfreq is the resonant frequency change, A is the area of the active surface, μq is an AT-cut quartz constant (2.947×10^{11} g/cm s^2), pq is the quartz crystal density (2.65 g/cm^3), and Fq is the reference frequency (9.04 MHz). The current efficiency of Cu electrodeposition at an applied current density of 5 ASD should be theoretically 100%,

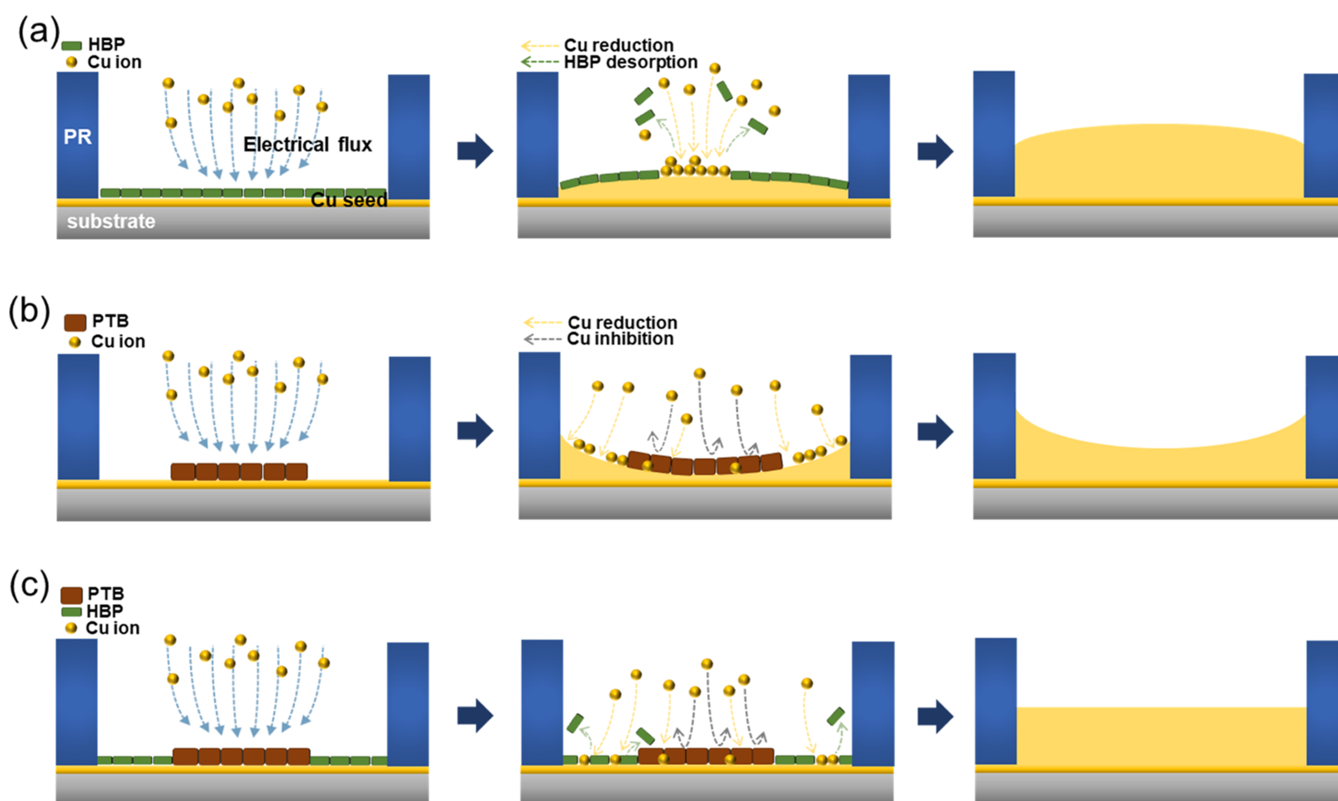

Figure 7. Schematics of shape variation in the electroplated Cu pillar by (a) HBP, (b) PTB, and (c) binary HBP + PTB.

since the standard reduction potential of Cu^{2+}/Cu (E^0 = 0.34 V) was much higher than that of $2H^+/H_2$ (E^0 = 0 V). Accordingly, the difference in mass change could be obtained in the presence of levelers, which went through the process sequence of adsorption/desorption and incorporation into Cu electrodeposition due to the fact that the Cu electrodeposition rate should be the same regardless of different levelers. As a consequence, the mass gain by adsorption of levelers was drawn from the difference in mass change between BS as a control and electrolytes containing levelers. Once 50 mA/cm^2 was applied, the adsorption rate was calculated to be 0.05 μg/s for HBP, 0.31 μg/s for PTB, and 0.36 μg/s for binary HBP + PTB, indicating that the mass change sequence was binary HBP + PTB > PTB > HBP. The higher change in mass in the presence of PTB could primarily be related to electrostatically sensitive adsorption, in view of the fact that the positively charged nitrogen of the quaternary pyridine ring was strongly adsorbed by the applied current. In contrast, it is likely that HBP was weakly adsorbed on the liquid−solid interface by the hydrophobic alkyl group rather than the adsorption of the pyridinium cation through electrostatic attraction.[28] Therefore, it was found that binary HBP + PTB exhibited the highest mass gain through the process of simultaneous adsorption, which could be explained by relatively uniform surface covering of HBP and the strong adsorption of PTB.

4. DISCUSSION

The results presented above exhibited that the coplanarity of the Cu pillars was affected by adsorption behaviors in the presence of HBP and PTB. Based on the molecular structures of HBP, as shown in Figures 1a and S5, the pyridine functional group could be partially changed to the pyridinium cation composed of positively charged nitrogen by the interactions of hydrogen ions, since pyridine and the pyridinium cation in acidic solution coexist in equilibrium.[29,30] In addition, HBP composed of the terminal $-CH_3$ of the alkyl group and the hydrophilic hydroxyl functional group played a role of the surfactant. Actually, the wettability of HBP was better than that of PTB, as evidenced by the results of a smaller contact angle on the PR and Cu seed layer (see Figure S6). Thus, it is believed that HBP was adsorbed on the Cu entire surface, although pyridinium partially formed from the interaction with hydrogen could be adsorbed on the Cu surface by electrostatic force. In the case of PTB, the pyridine ring has a consistently positive charge, unlike HBP (see Figure 1b). It should be noted that this unique structure, i.e., a positively charged quaternary pyridine ring, favored adsorption on the center of the Cu surface due to the electrostatic attraction.

The schematic illustrations of the different shapes of Cu pillars dependent on levelers are provided in Figure 7. On the basis of the similar surface roughness regardless of the measurement coordinates in the presence of HBP, it was found that the adsorption involving the hydrophobicity of the alkyl group was dominant rather than the electrostatically attracted adsorption by the formation of positively charged nitrogen. As represented by the potential change with RDE speed, HBP tended to be desorbed at a practical current density of 50 mA/cm^2. The small amount of almost identical nitrogen concentration (4−6 ppm within the error range) detected by SIMS and the lowest mass gain from EQCM further suggested that the desorption derived from weak adsorption occurred, as listed in Tables 1 and 2. HBP thus could exert an inhibitory effect even on the edge of the Cu seed layer, which is less sensitive to the electric field, but the growth of Cu deposition on the center region was inevitable due to the weak adsorption strength of HBP. As a result, a

https://doi.org/10.1021/acsomega.2c05646
ACS Omega 2022, 7, 36880−36887

Table 2. Nitrogen Concentrations in the Electroplated Cu Pillar

conditions	nitrogen concentration (ppm)	
	center of the Cu pillar	edge of the Cu pillar
BS	0	0
HBP	6	4
PTB	78	11
HBP + PTB	80	14

dome-like shape of Cu pillars could be obtained, as displayed in Figure 7a.

In contrast, PTB having quaternized nitrogen exhibited a substantially stronger adsorption nature relative to HBP consisting of pyrrolidine functionality. From the electrochemical studies, the potential of PTB was higher than that of HBP, and the potential change at a current density of 50 mA/cm^2 was not observable with increasing rotating disk speed. This suggests that the positively charged nitrogen migrated to the cathodic Cu surface by electrostatic attraction, and therefore, Cu deposition was strongly inhibited. Importantly, it was revealed that the nitrogen concentration of the center was much greater than that of the edge (see Table 2), indicating that an increase in the population of PTB at the center surface was correlated with the positively charged pyridine ring. This incorporation of a positively charged pyridine ring could contribute to the inhibitory effect at the center of the Cu deposit and result in a dish-like surface, as shown in Figure 7b.

In the case of HBP + PTB, the same potentials from chronopotentiometry were observed regardless of the injection sequence. This was likely due to the inhibitory effects of HBP and PTB originating from the complementary adsorption on the entire Cu seed layer and the center region. The measured *Ra* value and nitrogen concentration also indicated that HBP remained adsorbed on the edge of the Cu surface, whereas PTB was incorporated into the center by the following electric field pathway during the desorption of HBP from the center of the Cu surface. A binary leveler of HBP + PTB showed similar behaviors of individual HBP and PTB, which affected the synergistically inhibitory effect on the center and edge regions. Therefore, highly uniform Cu pillars could be formed, as shown in Figure 7c.

5. CONCLUSIONS

Cu pillars were electrodeposited on the Cu seed layer in a micropatterned photoresist in the presence of binary levelers of HBP and PTB with different functional groups. From electrochemical analysis, PTB composed of a positively charged pyridine ring was strongly adsorbed on the Cu seed surface, relative to HBP having an alkyl group with a hydrophobic nature. It was also revealed that the preferential adsorption of PTB on the center of the Cu seed derived from the electrostatic attraction, whereas the adsorption of HBP remained only at the edge region due to the desorption process on the center. Using binary HBP + PTB, the inhibitory effect on the entire surface contributed to uniform Cu deposition in contrast with the usage of a single leveler. Thus, it was concluded that the high coplanarity of the Cu pillars related to the adsorption behavior of binary levelers will substantially contribute to the high reliability of fine pitch bumps in the three-dimensional (3D) IC manufacturing field.

■ ASSOCIATED CONTENT

Supporting Information

The Supporting Information is available free of charge at https://pubs.acs.org/doi/10.1021/acsomega.2c05646.

Experimental details; measurement of the contact angle; profile of the PR patterned wafer; cross-sectional profile of the Cu pillar with various HBP and PTB compositions; EQCM graph; and molecular structures of pyridine and the pyridinium cation in acidic solution (PDF)

■ AUTHOR INFORMATION

Corresponding Authors

Sung-Min Kim − *Heat & Surface Technology R&D Department, Korea Institute of Industrial Technology (KITECH), Incheon 21999, Republic of Korea*; orcid.org/0000-0001-7490-5126; Email: sungminkim@kitech.re.kr

Sang-Yul Lee − *Department of Materials Engineering, Korea Aerospace University, Goyang 10540, Republic of Korea*; Email: sylee@kau.ac.kr

Min Hyung Lee − *Heat & Surface Technology R&D Department, Korea Institute of Industrial Technology (KITECH), Incheon 21999, Republic of Korea*; Email: minhyung@kitech.re.kr

Authors

Yugeun Jo − *Heat & Surface Technology R&D Department, Korea Institute of Industrial Technology (KITECH), Incheon 21999, Republic of Korea; Department of Materials Engineering, Korea Aerospace University, Goyang 10540, Republic of Korea*

SangHoon Jin − *Heat & Surface Technology R&D Department, Korea Institute of Industrial Technology (KITECH), Incheon 21999, Republic of Korea*

Woon Young Lee − *Heat & Surface Technology R&D Department, Korea Institute of Industrial Technology (KITECH), Incheon 21999, Republic of Korea*

Complete contact information is available at: https://pubs.acs.org/10.1021/acsomega.2c05646

Notes

The authors declare no competing financial interest.

■ ACKNOWLEDGMENTS

This research was supported by Basic Science Research Program through the National Research Foundation of Korea (NRF) funded by the Ministry of Education (2020M3H4A3081759).

■ REFERENCES

(1) Su, L.; Yu, X.; Li, K.; Pecht, M. Defect Inspection of Flip Chip Solder Joints Based on Non-Destructive Methods: A Review. *Microelectron. Reliab.* **2020**, *110*, No. 113657.

(2) Koh, W.; Lin, B.; Tai, J.*Copper Pillar Bump Technology Progress Overview*; ICEPT-HDP 2011 Proc. - 2011 International Conference Electronic Packaging Technology High Density Packaging, 2011; pp 1133−1137 DOI: 10.1109/ICEPT.2011.6067027.

(3) Luo, V.; Xue, X.-T.; Yu, K.-C.; Meng, J.; Lu, H.-L.; Zhang, D. W. Method to Improve the Process Efficiency for Copper Pillar Electroplating. *J. Electrochem. Soc.* **2016**, *163*, E39−E42.

(4) Castoldi, L.; Lodi, A.; Visalli, G. The Role of Organic Additives in the Localized Copper Plating: Flat, Dish, and Domed Shape Copper Bumps. *ECS Meet. Abstr.* **2008**, *MA2008-02*, 3160.

(5) Kim, B.; Ritzdorf, T.; Schmauch, D. Back-End Copper Metallization for Advanced Packaging: Bump, RDL, and TSV. *ECS Meet. Abstr.* **2006**, *MA2006-01*, 453.

(6) Chen, W.-C.; Huang, T.-T.; Lai, C.-H.; Chou, S.-W.; Shih, C.-H. Bump Shape Prediction of Cu Pillar via an Electrochemical Method. *ECS Trans.* **2013**, *52*, 453−460.

(7) Lee, P. T.; Chang, C. H.; Lee, C. Y.; Wu, Y. S.; Yang, C. H.; Ho, C. E. High-Speed Electrodeposition for Cu Pillar Fabrication and Cu Pillar Adhesion to an Ajinomoto Build-up Film (ABF). *Mater. Des.* **2021**, *206*, No. 109830.

(8) Li, L.-L.; Yang, C.-J. Size Control of Copper Grains by Optimization of Additives to Achieve Flat-Top Copper Pillars through Electroplating. *J. Electrochem. Soc.* **2017**, *164*, D315−D320.

(9) Gallaway, J. W.; Willey, M. J.; West, A. C. Acceleration Kinetics of PEG, PPG, and a Triblock Copolymer by SPS during Copper Electroplating. *J. Electrochem. Soc.* **2009**, *156*, D146.

(10) Tan, M.; Harb, J. N. Additive Behavior during Copper Electrodeposition in Solutions Containing Cl[Sup −], PEG, and SPS. *J. Electrochem. Soc.* **2003**, *150*, C420.

(11) Bandas, C. D.; Rooney, R. T.; Kirbs, A.; Jäger, C.; Schmidt, R.; Gewirth, A. A. Interfacial Leveler-Accelerator Interactions in Cu Electrodeposition. *J. Electrochem. Soc.* **2021**, *168*, No. 042501.

(12) Kim, H. C.; Choe, S.; Cho, J. Y.; Lee, D.; Jung, I.; Cho, W.-S.; Kim, M. J.; Kim, J. J. Bottom-up Filling of through Silicon Vias Using Galvanostatic Cu Electrodeposition with the Modified Organic Additives. *J. Electrochem. Soc.* **2015**, *162*, D109−D114.

(13) Dow, W. P.; Li, C. C.; Su, Y. C.; Shen, S. P.; Huang, C. C.; Lee, C.; Hsu, B.; Hsu, S. Microvia Filling by Copper Electroplating Using Diazine Black as a Leveler. *Electrochim. Acta* **2009**, *54*, 5894−5901.

(14) Wang, C.; Zhang, J.; Yang, P.; An, M. Electrochemical Behaviors of Janus Green B in Through-Hole Copper Electroplating: An Insight by Experiment and Density Functional Theory Calculation Using Safranine T as a Comparison. *Electrochim. Acta* **2013**, *92*, 356−364.

(15) Kobayashi, T.; Kawasaki, J.; Mihara, K.; Honma, H. Via-Filling Using Electroplating for Build-up PCBs. *Electrochim. Acta* **2001**, *47*, 85−89.

(16) Yang, S.; Thacker, Z.; Allison, E.; Bennett, M.; Cole, N.; Pinhero, P. J. Electrodeposition of Copper for Three-Dimensional Metamaterial Fabrication. *ACS Appl. Mater. Interfaces* **2017**, *9*, 40921−40929.

(17) Jin, S. H.; Kim, S. M.; Jo, Y.; Lee, W. Y.; Lee, S. Y.; Lee, M. H. Unraveling Adsorption Behaviors of Levelers for Bottom-Up Copper Filling in Through-Silicon-Via. *Electron. Mater. Lett.* **2022**, DOI: 10.1007/s13391-022-00364-6.

(18) Kim, S.; Marcano, M. C.; Becker, U. Effects of Hydroxyl and Carboxyl Functional Groups on Calcite Surface Wettability Using Atomic Force Microscopy and Density Functional Theory. *ACS Earth Space Chem.* **2021**, *5*, 2545−2554.

(19) Bozzini, B.; Mele, C.; Tadjeddine, A. Electrochemical Adsorption of Cyanide on Ag(1 1 1) in the Presence of Cetylpyridinium Chloride. *J. Cryst. Growth* **2004**, *271*, 274−286.

(20) Zhang, Y.; An, M.; Yang, P.; Zhang, J. Recent Advances in Electroplating of Through-Hole Copper Interconnection. *Electrocatalysis* **2021**, *12*, 619−627.

(21) Kim, J. J.; Kim, S. K.; Bae, J. U. Investigation of Copper Deposition in the Presence of Benzotriazole. *Thin Solid Films* **2002**, *415*, 101−107.

(22) Wang, A. Y.; Chen, B.; Fang, L.; Yu, J. J.; Wang, L. M. Influence of Branched Quaternary Ammonium Surfactant Molecules Aslevelers for Copper Electroplating from Acidic Sulfate Bath. *Electrochim. Acta* **2013**, *108*, 698−706.

(23) Kim, S. M.; Jin, S. H.; Lee, Y. J.; Lee, M. H. Design of Nickel Electrodes by Electrodeposition: Effect of Internal Stress on Hydrogen Evolution Reaction in Alkaline Solutions. *Electrochim. Acta* **2017**, *252*, 67−75.

(24) Qin, T.; Wang, Z.; Wang, Y.; Besenbacher, F.; Otyepka, M.; Dong, M.*Recent Progress in Emerging Two-Dimensional Transition Metal Carbides*; Springer: Singapore, 2021; Vol. *13* DOI: 10.1007/s40820-021-00710-7.

(25) Lee, M. H.; Lee, Y.; Oh, J. H.; Kim, Y. G.; Cho, S. K.; Kim, J. J. Microvia Filling with Copper Electroplated with Quaternary Ammonium-Based Leveler: The Evaluation of Convection-Dependent Adsorption Behavior of the Leveler. *J. Electrochem. Soc.* **2017**, *164*, D1051−D1055.

(26) Lee, M. H.; Kim, M. J.; Kim, J. J. Competitive Adsorption between Bromide Ions and Bis(3-Sulfopropyl)-Disulfide for Cu Microvia Filling. *Electrochim. Acta* **2021**, *370*, No. 137707.

(27) Kankare, J. Sauerbrey Equation of Quartz Crystal Microbalance in Liquid Medium. *Langmuir* **2002**, *18*, 7092−7094.

(28) Lv, J.; Zhao, X.; Jie, X.; Li, J.; Wei, X.; Chen, B.; Hong, G.; Wu, W.; Wang, L. Fatty Acid Quaternary Ammonium Surfactants Based on Renewable Resources as a Leveler for Copper Electroplating. *ChemElectroChem* **2019**, *6*, 3254−3263.

(29) Ekimova, M.; Kubin, M.; Ochmann, M.; Ludwig, J.; Huse, N.; Wernet, P.; Odelius, M.; Nibbering, E. T. J. Soft X-Ray Spectroscopy of the Amine Group: Hydrogen Bond Motifs in Alkylamine/Alkylammonium Acid-Base Pairs. *J. Phys. Chem. B* **2018**, *122*, 7737−7746.

(30) Brenlla, A.; Veiga, M.; Pe, J. L.; Carmen, M. R.; Rodr, F.; Mosquera, M. Photoinduced Proton and Charge Transfer in 2-(2′-Hydroxyphenyl)Imidazo[4,5-b]Pyridine. *J. Phys. Chem. B* **2013**, *117*, 884−896.

https://doi.org/10.1021/acsomega.2c05646
ACS Omega 2022, 7, 36880−36887